Modulational instability in a twin-core fiber with the effect of saturable nonlinear response and coupling coefficient dispersion

K. Nithyanandan,[1] R. Vasantha Jayakantha Raja,[2] and K. Porsezian[1]
[1]*Department of Physics, Pondicherry University, Pondicherry 605 014, India*
[2]*Department of Physics, Central University of Tamil Nadu, Thiruvarur, India*
(Received 7 November 2012; published 4 April 2013)

Modulational instability (MI) in a twin-core optical fiber with the combined effect of saturation of nonlinearity (SNL) and coupling coefficient dispersion (CCD) is presented. The CCD does not dramatically modify the spectrum of the symmetric or antisymmetric continuous wave (CW) case, but the SNL on the other hand behaves in a perceptible manner such that the gain and the unstable region inherently decrease. In the anomalous dispersion region, the gain of the instability spectrum increases (decreases) monotonously with power (coupling coefficient). The effective nonlinearity and the power threshold for the sustained CW solution becomes a function of power for the SNL case. The so-called nonlinear factor behaves in a unique way such that there exist two powers for the same value of nonlinear factor. The interplay between CCD and SNL is emphasized, where any nonzero value of CCD leads to new instability bands and the saturation on the other hand suppresses the gain of the instability band. We identified a pair of power corresponding to the constant value of the nonlinear factor, where the system becomes invariant, such that the number of instability bands, the gain, and the range of the unstable region are all preserved. In the case of the normal dispersion case, the MI is achieved purely by means of the coupling coefficient. In both cases, a critical CCD is predicted, where the system evolves dramatically in a different manner.

DOI: 10.1103/PhysRevA.87.043805 PACS number(s): 42.65.−k, 42.79.Gn

I. INTRODUCTION

The interaction between the natural phenomena such as the linear dispersion due to the frequency-dependent refractive index and the nonlinearity due to the intensity-dependent refractive index generates interesting features which has aroused a great deal of interest both from the fundamental point of view as well as the applications perspective [1,2]. The stability of the input light beam under various physical situations is one of the most exciting issues of modern nonlinear optics. One such exciting prospect that deserves renowned interest is the so-called modulational instability. The MI is a universal instability process which is identified as a characteristic of wave propagation in dispersive nonlinear systems, such as fluid dynamics [3], nonlinear optics [4], and plasma physics [5]. In the context of nonlinear optics, the MI can be explained as the continuous wave (CW) or quasi-CW propagating in the nonlinear dispersive medialike optical fibers, becoming inherently unstable under weak perturbation and evolving into a train of ultrashort pulses as a consequence of temporal modulation due to MI.

The history of the MI dates back to the mid-1960s, courtesy of Lighthill, who is responsible for the famous Lighthill criterion which sets the conditions for the stability of the plane wave in a nonlinear dispersive medium [6]. Such an instability condition later in the name of MI was observed first in hydrodynamics by Benjamin and Feir in 1967 [3]. In the same year, Ostrovskii predicted the possibility of MI in nonlinear optics [7] and this was later explained in detail by Hasegawa *et al*. in 1973 in the context of optical fibers [8]. Ever since these pioneering works, MI picks momentum and evolves as one of the most fascinating phenomena in the field of nonlinear optics. The sweeping interest of MI for more than five decades in various disciplines of science and technology is a clear manifestation about the everlasting interest of MI in the exciting fields of research such as in optical communications and signal processing systems, ultrafast pulse generation, supercontinuum generation [9,10], new laser sources [11,12], all-optical switching [13,14], optical amplification of weak signals, material absorption and loss compensations, etc. [14–16]. MI, over the years has been systematically investigated in connection with numerous nonlinear processes. In principle, MI can be classified as temporal or longitudinal MI [1,8,17] or spatial or transverse MI [18,19] based on the linear part of the system, depending on whether the CW wave disperses or diffracts in the nonlinear medium. The spatiotemporal MI has also been observed, especially in the bulk media when both dispersion and diffraction act simultaneously [19,20].

The MI is governed by the nonlinear Schrödinger equation (NLSE), which inherently admits the formation of solitary pulses or envelope solitons as a result of the delicate balance between the anomalous group velocity dispersion (GVD) and the self-focusing Kerr nonlinearity [1,8,17]. The periodic pulse trains that emerge as the result of the temporal modulation due to MI is in fact identified as the train of the ideal soliton pulses. This emphasizes the close relation between MI and soliton and hence, at times, MI is called as a soliton precursor. The MI in the conventional dispersive nonlinear media has been widely studied. The MI scenario in photorefractive media has been studied in detail by Staffman *et al*. [21]. In general, MI occurs in the anomalous group-velocity dispersion (GVD) regime for a self-focusing nonlinearity and results in the symmetrical pair of side bands corresponding to the Stoke's and anti-Stoke's component. However, the domain of MI can be extended to the normal GVD regime, under some special cases, such as in the presence of higher even-order linear dispersions, typically fourth-order dispersion [22–24], or loss dispersion [25], in the case of co-propagation of two or more optical fields in the optical fiber as in the case of cross-phase modulation instability [26,27] and polarization modulation instability [28,29].

Following the detailed introduction with historical perspectives, we are now moving on to the objective of the paper. Ever since the discovery of the nonlinear directional coupler by Jensen, there has been profound interest in the study of the nonlinear directional coupler in various applications such as ultrafast optical switching, wavelength division multiplexing, power splitters, optical logic gates, multifrequency generation or supercontinuum generation, etc. [30–35]. The study of MI in the nonlinear directional coupler or the dual core fiber is not new, since a good amount of research work has been dedicated to understand the MI dynamics in such a fiber system. For instance, Trillo *et al*. in 1988 analyzed extensively the impact of various combinations of physical effects in the MI dynamics of the nonlinear directional coupler and studied the close relation between the MI in two-core fibers and the birefringent glass fibers. Along similar lines, Tasgal *et al*. extended study to the case of an asymmetric dual-core optical fiber and analyzed the MI with reference to the bifurcation point [36].

The evolution of the optical beam in the twin-core fiber is given by a pair of linearly coupled nonlinear Schrödinger equations [37–39]. The periodic power transfer between the two cores of the fiber is governed by the linear coupling coefficient [40,41]. However, in the ultrashort pulse regime, the so-called CCD arising as a result of the wavelength-dependent coupling coefficient is found to be crucial [42–44] especially in long fibers and can cause severe pulse distortion, which eventually leads to pulse break-up [45,46]. The effect of CCD and its relative influence on various physical mechanisms was studied in detail both theoretically and also through experiments by Chiang and his group through various analysis [37–39,42,43,46]. Considering the importance of CCD, Li *et al*. extended the results of Refs. [14,36] with the inclusion of CCD [47]. The authors have reported that CCD does not affect the symmetric or asymmetric CW state but dramatically changes the MI of the asymmetric CW state. Over the years the perception of analyzing MI in a two-core fiber system takes a different dimension based on the linear and nonlinear contribution of the refractive index of the medium. One such interesting prospect is the study of the saturation of nonlinear response in the propagation dynamics of two-core fibers [48–52]. In principle, for any material medium, there is an upper limit for the optically induced nonlinear refractive index, beyond which the higher-order nonlinear susceptibilities inevitably get excited and after a certain power threshold the nonlinear response saturates [53,54]. In particular, a fiber system such as semiconductor doped fibers, and the modern nonsilica technology such as SF6, TF10, CS_2, or nitrobenzene-filled photonic crystal fibers, possesses nonlinearity approximately 200 times larger than the conventional silica-based fiber system and hence the nonlinear saturation occurs even at a moderate power level. In recent times, the liquid core photonic crystal fibers deserve considerable interest especially in the context of soliton propagation due to its high nonlinearity and requirement of low input pulse energy [55–58]. Similarly, dual core photonic crystal fibers with selective liquid filling have also found serious interest in wide application [59]. Although a good number of works involving the study of saturation in the propagation dynamics of the two-core fiber system have been reported, no convincing report to the best of our knowledge is available in the study of saturation of nonlinear response in the context of MI in two-core fibers. However, the study of MI in SNL is not novel as one can see from Refs. [60–62], but what differentiates our present problem from the rest is the investigation of MI in two-core fibers with the effect of saturation and the interplay between the CCD, which has not been discussed yet to our knowledge and hence deserves attention. Thus the end of the article will discuss the characteristic properties of MI with the effect of SNL in two-core fibers and the interplay between the SNL and CCD.

II. THEORETICAL MODEL

The propagation of a high intense optical beam in the single-mode twin-core fiber in the limit of a slowly varying envelope approximation is given by the pair of linearly coupled nonlinear Schrödinger equations (CNLSE). The CNLSE describing the evolution of the slowly varying envelopes (U_j, $j = 1,2$) with the effect of SNL is given by the equation as follows [47–52]:

$$i\frac{\partial U_j}{\partial z} - \frac{1}{2}\beta_2\frac{\partial^2 U_j}{\partial t^2} + \kappa\, U_{3-j} + i\kappa_1\frac{\partial U_{3-j}}{\partial t} + \gamma\frac{f(\Gamma|U_j|^2)}{\Gamma}U_j = 0, \tag{1}$$

where $t = (\tau - \beta_1 z)$ is the retarded time and z is the longitudinal coordinate. The group velocity is given by β_1 and β_2 is the group velocity dispersion parameter. The nonlinear Kerr coefficient (γ) is of the form $\gamma = \frac{n_2\omega_0}{cA_{\text{eff}}}$, where ω_0 is the carrier frequency, n_2 is the nonlinear index coefficient, and A_{eff} is the effective core area. The coefficient of linear coupling is given by κ, and $\kappa_1 = d\kappa/d\omega$ is the coupling coefficient dispersion due to the wavelength dependence of κ.

The function $f(\Gamma|U|^2)$ describes the intensity-dependent refractive index. In principle, all nonlinearities saturate, that is, there is an upper limit in all optical materials for the refractive index change that can be induced optically and a further rise in power does not modify the nonlinear refractive index. At a higher input power level, higher-order nonlinear susceptibilities inevitably get excited which eventually leads to the saturable behavior. In addition, it is reported in Ref. [63], that the saturation of cubic nonlinearity is equivalent to the presence of higher-order nonlinearities as a result of $\chi^{(3)}$ $\chi^{(5)}$ and $\chi^{(7)}$. Thus, we stick to the case of saturation of cubic nonlinearity as it is the most practical model representing saturable nonlinearity [48–52]. It is quite understandable that, in most nonlinear liquids, as the input power reaches a certain level, the photon energy certainly tends to approach the absorption edge, which leads to ultimate large nonlinear absorption. As it is well known that MI stems on the optical nonlinearities and the associated pump power of the system, any detrimental effects such as nonlinear absorption is quite serious and will lead to undesirable features (i.e., inhibits the MI as a result of the depletion of pump power due to nonlinear absorption and subsequently suppresses the gain and the side-band growth). In order to overcome the above penalizing factor, the considered twin-core fiber system is assumed to be transparent for the input carrier frequencies (i.e., the input carrier energy is below the band gap of the fiber material and it is not in resonance with impurity trap levels or any other energy level of the fiber system). This is indeed

a valid assumption, since it takes into account only the real part of the higher-order nonlinear susceptibilities and keeps away the contribution from the imaginary part. The resulting functional form of the saturable nonlinear response that is commonly used in the literature in the context of the nonlinear directional coupler is given by

$$f(\Gamma|U|^2) = 1 - \exp(-\Gamma|U|^2), \tag{2}$$

where Γ is the saturation parameter of the form $\Gamma = 1/P_s$, and P_s is the power corresponding to the nonlinear saturation. The other empirical forms of saturable nonlinearity can be seen from Refs. [24,61,62].

The pertinent equation incorporating the above assumption leads to the modified coupled nonlinear Schrödinger equation (mCNLSE) of the form as follows:

$$i\frac{\partial U_j}{\partial z} - \frac{1}{2}\beta_2\frac{\partial^2 U_j}{\partial t^2} + \kappa\, U_{3-j} + i\kappa_1\frac{\partial U_{3-j}}{\partial t} + \gamma\frac{1-\exp(-\Gamma|U_j|^2)}{\Gamma}U_j = 0. \tag{3}$$

It is worth noting that the above equation governing the dynamics of MI in the two-core fiber system switches back to the conventional Kerr case when the field intensity $\Gamma|U|^2 \ll 1$. Thus for low-input intensity the Kerr-type nonlinear response is more pronounced. Considering all the above-mentioned critical points, we study the mechanism of MI in the twin-core LCPCF in the saturation windows of nonlinear response.

III. LINEAR STABILITY ANALYSIS

A. Symmetric and antisymmetric solutions

The fundamental framework of MI analysis relies on the linear stability analysis (LSA), such that a CW solution is perturbed by a small amplitude or phase perturbation satisfying the condition $|a_j(z,t)|^2 \ll |P_0|^2$, and then study whether the perturbation amplitude grows or decays with propagation.

The symmetric or antisymmetric CW steady-state solution can be written as

$$U_1^{\mathrm{CW}} = P_0\exp[i\phi(z)], \quad U_2^{\mathrm{CW}} = \delta P_0\exp[i\phi(z)], \tag{4a}$$

where P_0 is the input pump power and ϕ is the nonlinear phase shift.

$$\phi(z) = (\gamma\tilde{P}_0 + \delta\kappa)z, \tag{4b}$$

with $\tilde{P}_0 = (\frac{1-e^{-\Gamma P_0}}{\Gamma})$ and $\delta = +1\ (-1)$ corresponding to symmetric or antisymmetric solutions.

The stability of the steady state can be examined by introducing a perturbed field $q_j(z,t)$ of the form,

$$U_j^P = [P_0 + q_j(z,t)]\exp[i\phi(z)]. \tag{5}$$

The linearized equation for the perturbation can be obtained by using Eq. (5) in Eq. (3) and neglecting the higher-order perturbation terms as follows:

$$i\frac{\partial q_j}{\partial z} - \frac{1}{2}\beta_2\frac{\partial^2 q_j}{\partial t^2} + \kappa\,(q_{3-j} - \delta\, q_j) + i\kappa_1\frac{\partial q_{3-j}}{\partial t} + \tilde{\gamma}\,P_0(q_j + q_j^*). \tag{6}$$

The following ansatz is assumed for the perturbation with frequency detuning from the pump Ω, and K will be the wave number of the perturbation.

$$q_j(z,t) = U_j\exp[-i(Kz - \Omega t)] + V_j\exp[i(Kz - \Omega t)], \tag{7}$$

where U_j and V_j are the perturbation amplitudes of anti-Stokes and Stokes side bands, respectively. Using Eq. (7) in Eq. (6) results in four homogenous equations for U_j and V_j.

The compatibility condition for two equations in U_1 and V_1 lead to the dispersion relation as follows:

$$(K - \delta\kappa_1\Omega)^2 = \tfrac{1}{4}\beta_2\Omega^2(\beta_2\Omega^2 + 4\tilde{\gamma}P_0). \tag{8}$$

However, for U_2 and V_2 the compatibility condition deviates from the earlier one due to linear coupling between the modes and the dispersion relation is of the form,

$$(K + \delta\kappa_1\Omega)^2 = \tfrac{1}{4}(\beta_2\Omega^2 - 4\delta\,\kappa)(\beta_2\Omega^2 - 4\delta\kappa + 4\tilde{\gamma}P_0). \tag{9}$$

The resulting general relation corresponding to the stability of the steady-state solution of the two-core fiber system can be written as

$$[(K - \delta\kappa_1\Omega)^2 - h_1][(K + \delta\kappa_1\Omega)^2 - h_2)] = 0. \tag{10}$$

$$h_1 = \tfrac{1}{4}\beta_2\Omega^2(\beta_2\Omega^2 + 4\tilde{\gamma}P_0), \tag{11a}$$

$$h_2 = \tfrac{1}{4}(\beta_2\Omega^2 - 4\delta\kappa)(\beta_2\Omega^2 - 4\delta\kappa + 4\tilde{\gamma}P_0), \tag{11b}$$

$$\tilde{\gamma} = \gamma e^{-\Gamma P_0}. \tag{11c}$$

As it is well known that the MI is said to occur only for the nonzero imaginary part of K and the amplitude perturbation grows with propagation with a gain given by $\mathrm{Im}[K]$. This can be achieved by either $h_1 < 0$ or $h_2 < 0$; this is possible only when the dispersion coefficient takes a negative value. However, the presence of the linear coupling coefficient in the dispersion relation satisfies the condition of the nonzero imaginary part for the wave vector and thereby extends the domain of MI to the normal dispersion regime.

A more comprehensive theoretical analysis featuring the role of saturation of nonlinear response in the instability spectra of the twin-core fiber system in the absence of CCD can be seen from Refs. [2,14,36]. As we are interested in studying the interplay between CCD and κ_1, it is observed that in the case of the symmetric or antisymmetric case the CCD (κ_1) does not have much impact on MI dynamics (no change in the gain) and SNL on the other hand hardly does much, apart from suppressing the MI [61,62]. The intermodal dispersion does not have much effect, since only one supermode corresponding to symmetric (even supermode) or antisymmetric (odd supermode) exists. [47]. Thus we conclude from this section that the role of CCD in the symmetric or antisymmetric solution is found to be insignificant and the saturation on the other hand behaves very much in a perceptible manner as it is published elsewhere [24,60,61] and hence will not be discussed.

B. Asymmetric solutions

Along similar lines with the symmetric or antisymmetric CW solution, the so-called asymmetric CW solution can be obtained as follows:

$$U_1^{\mathrm{CW}} = P_1\exp[i\phi(z)], \quad U_2^{\mathrm{CW}} = P_2\exp[i\phi(z)]. \tag{12}$$

The nonlinear phase shift $\phi(z)$ can take the form $\phi(z) = \gamma(\tilde{P}_1 + P_2)z = \gamma P z$, with $\tilde{P}_1 = (\frac{1-e^{-\Gamma P_1}}{\Gamma})$. It is worth noting that our calculation is in agreement with the report of Ref. [47] at the limiting case of the Kerr-type nonlinear response.

There exists a minimum power threshold to sustain the CW solution for a given κ. The power threshold is found to be $P_{\min} = 2\kappa/\tilde{\gamma}$ and at $P_{\min}$ the system switches back to the symmetric CW state. Following a similar procedure for linear stability analysis as in the preceding section, the dispersion relation after some mathematical manipulations can be written as

$$\left[\left(K + \frac{\kappa_1 \Omega}{\sqrt{2}}\right)^2 - h_1\right]\left[\left(K + \frac{\kappa_1 \Omega}{\sqrt{2}}\right)^2 - h_2\right] = h, \quad (13)$$

$$h_1 = \frac{1}{2}\left[\tilde{\gamma}^2 P^2 - 4\kappa^2 + \left(\kappa_1^2 - 2\sqrt{2}\beta_2\kappa\right)\Omega^2 + \frac{\beta_2^2\Omega^4}{2}\right], \quad (14a)$$

$$h_1 = \frac{1}{2}\left[\tilde{\gamma}^2 P^2 - 4\kappa^2 + \left(\kappa_1^2 + 2\sqrt{2}\beta_2\kappa\right)\Omega^2 + \frac{\beta_2^2\Omega^4}{2}\right], \quad (14b)$$

$$h = \frac{1}{4}(\tilde{\gamma}^2 P^2 - 4\kappa^2)^2 - (\tilde{\gamma}^2 P^2 - 4\kappa^2)\left(\beta_2\tilde{\gamma} P + 2\kappa_1^2\right)\Omega^2 - \left(5\beta_2^2\kappa^2 + \kappa_1^4 - \beta_2^2\tilde{\gamma}^2 P^2\right)\Omega^4 + \frac{1}{2}\beta_2^2\kappa_1^2\Omega^6, \quad (14c)$$

$$\tilde{\gamma} = \gamma \exp^{-\Gamma P}. \quad (14d)$$

The MI gain spectra are given by the relation $G(\Omega) = 2\,\mathrm{Im}[K]$ and it is observed that the spectrum is symmetrical $G(\Omega) = G(-\Omega)$ across the center frequency; therefore, we prefer to show only the positive side of the spectrum for better illustration. In what follows, we consider the nonlinear parameter and dispersion coefficient as $\gamma = 3.05\ \mathrm{kW^{-1}m^{-1}}$, $\beta_2 = \pm 0.02\ \mathrm{ps^2 m^{-1}}$. The saturation power is assumed to be $P_s = 100$ kW and the operating input power varies in the range $P = 0 - 200$ kW. The coupling coefficient and the coupling coefficient dispersion varies, respectively, in the range $\kappa = 0 - 25\ \mathrm{m^{-1}}$ and $\kappa_1 = 0 - 10\ \mathrm{ps\ m^{-1}}$. It should be noted that the above set of parameters will be used all through our analysis and will not be specified always, unless and until any change in the choice of the parameters. We have chosen alphabets $A < B < C < D < E < F$ for variables in the plots based on the increasing order of the numerical value (a similar pattern is followed for the choice of the colors in the figures and will be maintained throughout the discussion).

IV. MODULATIONAL INSTABILITY ANALYSIS

Following the detailed mathematical treatment pertaining to the MI dispersion relation corresponding to the two-core system with the effect of SNL. The subsequent section is intended to provide an insight analysis about the interplay between the CCD and SNL in the MI dynamics. In order to provide a comprehensive picture, we consider both the dispersion regime, namely, anomalous and normal dispersion regime. The analysis is documented in such a way that in addition to the exclusive investigation about the interplay between SNL and CCD, an interactive discussion will be emphasized between the SNL and the conventional Kerr case, so as to explore the impact of saturation in the MI dynamics of the two-core fiber system in the presence of CCD.

A. Anomalous dispersion regime

The anomalous dispersion regime corresponds to the case where the dispersion coefficient β_2 takes a negative value, and the MI is said to occur due to the interplay between the self-focusing nonlinearity and the negative group dispersion coefficients, which results in the growth of the weak perturbation and eventually leads to the breakup of the CW into a train of solitonlike pulse trains.

To put things in a self-explanatory way, before dealing with the interplay between CCD and SNL, it is more instructive to investigate the impact of pump power and the coupling coefficient in the MI dynamics of the SNL system without the effect of CCD.

1. Impact of pump power in the MI spectrum

To give a quantitative picture of the impact of pump power in the SNL system, the gain spectrum of MI as a function of pump power is studied.

(a) First, the MI spectrum corresponding to the conventional Kerr case is considered by making $\Gamma \to 0$. Figure 1 shows the MI gain spectrum as a function of power and one can straightforwardly notice from the contour map that the MI gain monotonously increases with the power.

(b) Now we incorporate the saturation into the picture and therefore the effective nonlinear coefficient becomes $\gamma \to \tilde{\gamma}$. The MI gain spectrum as a function of power is shown in Figs. 2(a) and 2(b). Basically, we divided the operating power into two regimes with reference to the saturation power. For instance, without loss of generality, the saturation power (P_s) is set to be equal to 100 kW, thus the saturation parameter Γ becomes $0.01\ \mathrm{kW^{-1}}$. We classified the operating power regime as Type I and Type II corresponding to the pumping at below saturation power ($P > P_s$) or above saturation power ($P > P_s$), respectively. The corresponding MI spectrum as a function of power is shown in Figs. 2(a) and 2(b). The behavior of the

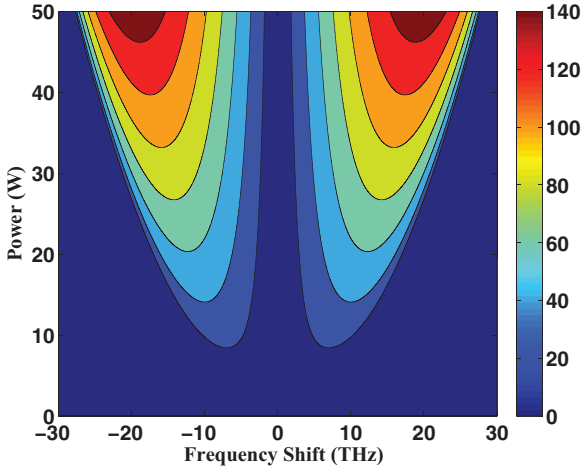

FIG. 1. (Color online) The MI gain spectra in the anomalous dispersion regime as a function of input power. Parameters are $\beta_2 = -0.02\ \mathrm{ps^2 m^{-1}}$, $\gamma = 3.05\ \mathrm{kW^{-1}m^{-1}}$, $\kappa = 10\,\mathrm{m^{-1}}$.

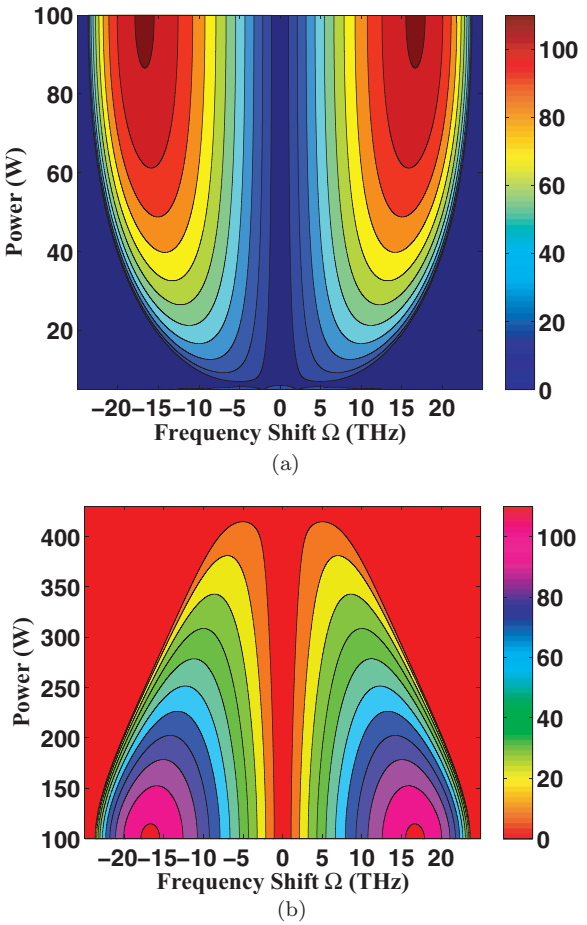

FIG. 2. (Color online) Plot showing the variation of MI gain spectra of SNL as a function of input power at $\Gamma = 0.01\text{W}^{-1}$. (a) MI spectrum at Type-I regime. (b) MI spectrum at Type-II regime.

MI gain spectrum in the Type-I regime for different power is shown in Fig. 2(a) and resembles in principle the one obtained for the conventional Kerr-type nonlinear response, that is, the MI gain increases nearly monotonously with power. On the contrary, the behavior of MI gain for different powers in the Type-II regime is interesting, since the power-gain relation is exactly opposite to the case of the conventional Kerr response [i.e., instead of increasing with power, the MI gain decreases with increase in power as shown in Fig. 2(b)].

The aforementioned interesting behavior of pump power is identified to be unique in the context of MI, such that the increasing power either increases or decreases the MI gain relative to the saturation power. For the better illustration and to give insight in the view of understanding the unusual observation of the role of pump power in the SNL system, we studied the impact of different parameters as a function of power. First, the nonlinear coefficient as a function of power is drawn for different saturation parameters as shown in Fig. 3(a). It is observed that for the case of the Kerr-type nonlinear response the effective nonlinear coefficient becomes $\tilde{\gamma} \to \gamma$ and it is found that the variation of the effective nonlinear coefficient is independent of the input power.

On the other hand, the nonlinear coefficient in the SNL system is found to be a sensitive function of the power and γ decreases with an increase in the pump power. It is obvious from Fig. 3(a) that as the saturation parameter increases (curve C), the nonlinear coefficient $\tilde{\gamma}$ decreases very rapidly. Since the nonlinear coefficient decreases unusually with increases in power, it opens the possibility that there must exist an interesting relation between the effective nonlinearity and the input power. To account for that, we have plotted the product of nonlinear coefficient and power as a function of power and we called it the nonlinear factor. It is evident from Fig. 3(b), that the nonlinear factor increases with power for power $P < P_s$ (i.e., Type I reaches a maximum at $P = P_s$ and decreases with further increase in power, Type II for $P > P_s$, whereas the nonlinear factor corresponding to the conventional Kerr case increases monotonously [curve A of Fig. 3(b)]. The nature of the curve for the case of SNL in Fig. 3(b) illustrates that there exist two pump powers for the same value of the nonlinear factor. Since, the nonlinear factor is identified to be a crucial determining factor, hence an insight analysis is expected to be useful. To demonstrate, an arbitrary line corresponding to the nonlinear factor 100 m^{-1} is drawn across the curve and the line bisects the curve at two points, which corresponds to two powers—one at the Type-I regime (59.45 kW) and the other at the Type-II regime (155.7 kW). It is interesting to note that for each value of nonlinear factor there exists a set of power corresponding to one at the Type-I regime ($P < P_s$) and the other at the Type-II regime ($P > P_s$). It is noteworthy that the system behaves similarly in the two different powers. The MI gain spectrum related to the two input powers, 59.45 kW and 155.7 kW, respectively, is shown in Fig. 4 alongside the conventional Kerr case. Unarguably, the MI gain of the SNL system is less than the conventional Kerr case, which is attributed to the inherent depletion in the

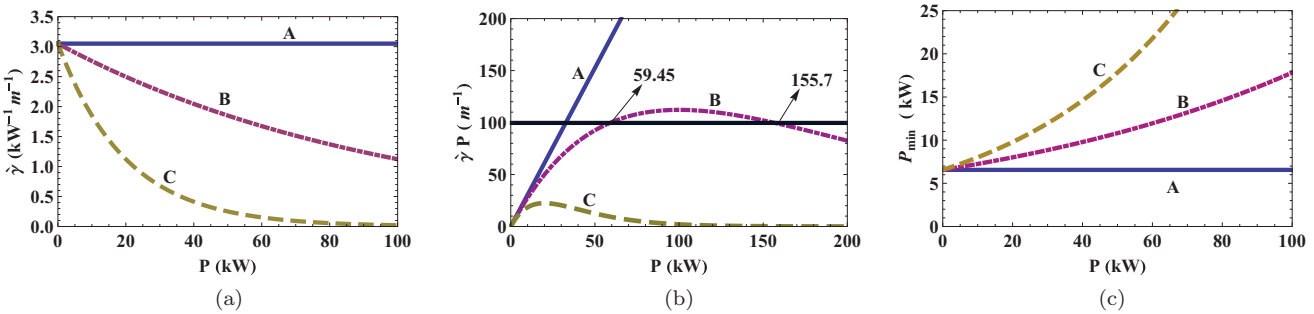

FIG. 3. (Color online) Plot showing the variation of the system parameter as a function of power. (a) Nonlinear coefficient as a function of power. (b) Nonlinear factor as a function of power. (c) P_{min} as a function of power.

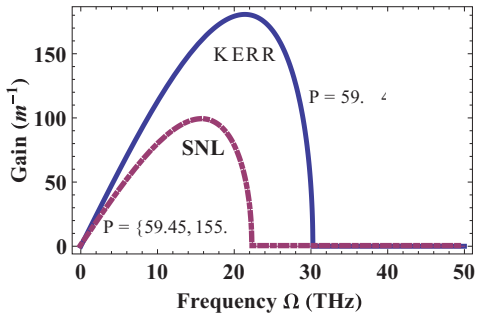

FIG. 4. (Color online) The instability spectra of the Kerr and SNL system corresponding to a nonlinear factor equals 100 m^{-1}.

effective nonlinearity ($\tilde{\gamma}$) of the SNL system. Interestingly, one could not differentiate (appears as if a curve for a single power) the curves corresponding to the two different powers (59.45 kW and 155.7 kW) which is identified as the signature of the SNL system.

In this conjecture, it is worth saying that the behavior of the SNL system is indeed interesting, such that the system becomes invariant at two different powers (one at Type I and other at Type II) for a constant nonlinear factor. We speculate the aforementioned observation as interesting and can be useful in many circumstances. As it is known that the nonlinear coefficient depends on the input power in the SNL, the so-called $P_{\min}$, which is a certain function of the nonlinear coefficient also depends on the input power, whereas in the conventional case the $P_{\min}$ is independent of the input power (curve A) as shown in Fig. 3(c).

2. *Variation of MI spectrum with kappa*

The influence of the coupling coefficient κ in the MI spectrum of the SNL system is shown in Fig. 5. Figure 5 is plotted for different κ at a constant power ($P = 20$ kW). It is straightforward to notice that as κ increases the $G_{\max}$ decreases and the maximum gain is achieved for the uncoupled case ($\kappa = 0$).

3. *Interplay between saturation and coupling coefficient dispersion in the MI spectrum*

Following the understanding of the role of the pump power and κ in the instability spectrum of the SNL system, the featuring section is dedicated exclusively to the investigation

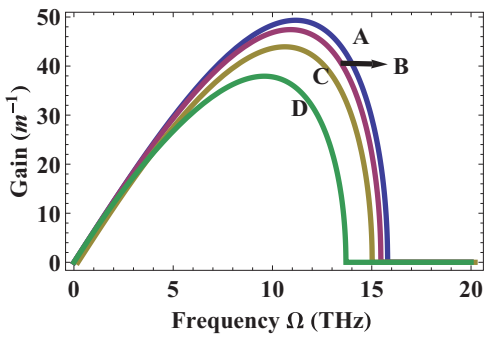

FIG. 5. (Color online) The MI spectra of SNL at $\kappa(A = 5; B = 10; C = 15; D = 20)$ m^{-1} for power $P = 20$ kW.

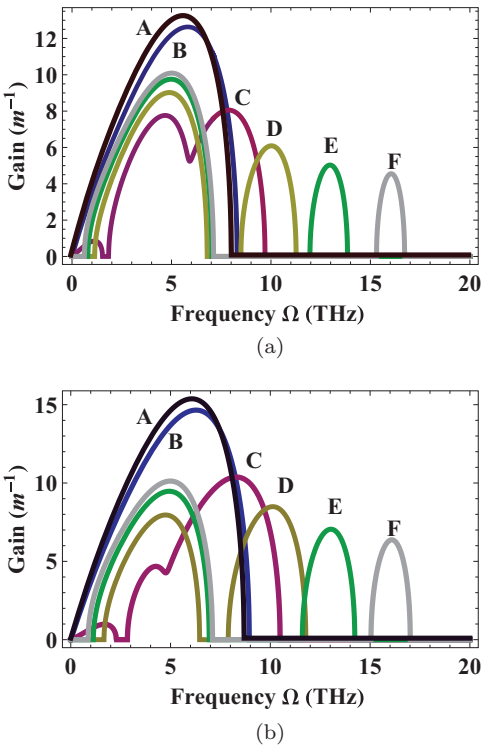

FIG. 6. (Color online) Plot showing the instability spectra at $P = 8$ kW for different coupling coefficient dispersions $\kappa_1(A = 0; B = -0.2; C = -0.45; D = -0.6; E = -0.8; F = -1)$ ps m^{-1}. (a) The MI spectra of Kerr at low power with the effect of coupling coefficient dispersion (κ_1). (b) The MI spectra of SNL at low power with the effect of coupling coefficient dispersion (κ_1).

of the interplay between saturation and coupling coefficient dispersion. For better illustration, the conventional Kerr case is considered alongside our purported SNL case. The choice of the parameters is defined by ensuring a sustained CW solution in the system. We fix the coupling coefficient $\kappa = 10$ m^{-1}, and the calculated power threshold for sustained CW is found to be 6.55 kW and 7.10 kW, corresponding to the conventional and SNL system, respectively. It is straightforward to notice that the incorporation of saturation increases the $P_{\min}$. In similar lines with Ref. [47], we consider two power schemes (should not be confused with Type I and Type II of the SNL system), one at or near $P_{\min}$ and the other at far from $P_{\min}$, typically 7 and 20 kW for the conventional case and 8 and 20 kW for the SNL case.

For instance, we begin the discussion by considering the low power case (i.e., pumping slightly above the $P_{\min}$, 8 kW. Figures 6(a) and 6(b) depict the instability spectrum corresponding to the conventional Kerr and SNL cases for some representative value of CCD. It is apparent that both systems closely resemble each other, and the notable difference is the range of the unstable frequency and the gain of the instability band. It is obvious from Figs. 6(a) and 6(b) that at zero CCD, there exists a single band of maximum gain at the center frequency. Although our strategic view is on the role of CCD in the MI spectrum of the SNL system, an interactive comparison will be made with the conventional counterpart for a better understanding. From Fig. 6(b), one can observe that as CCD increases (scaled by the parameter κ_1), the instability

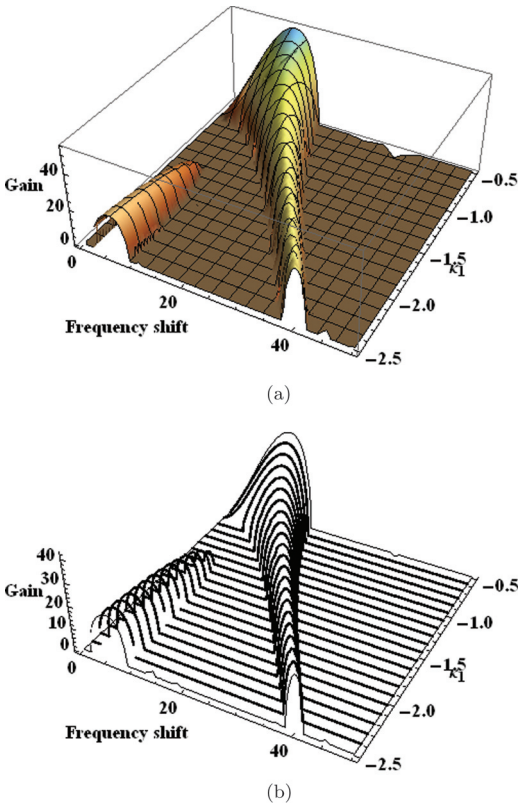

FIG. 7. (Color online) Plot showing the instability spectra at $P = 20$ kW for different coupling coefficient dispersions. (a) The MI spectra of Kerr at high power with the effect of coupling coefficient dispersion (κ_1). (b) The MI spectra of SNL at high power with the effect of coupling coefficient dispersion (κ_1).

band drifts slightly towards the higher detuning frequencies and the gain of the primary band (instability band near the center frequency) decreases. With further increase in CCD, it is observed that there exists a critical CCD at which a new instability band appears near the center frequency whose gain increases and eventually saturates for a higher value of κ_1. On the hand, there appears a secondary band at higher detuning frequency as soon as the CCD crosses the critical limit $|\kappa_1|$. The gain of the secondary band at higher detuning frequency decreases with an increase in the CCD as shown in Fig. 6(b) for different values of CCD. The significant difference between the conventional and SNL case is observed to be the critical value of CCD, where κ_1 in SNL is higher than that of the conventional Kerr case.

Now we switch to the case of input power higher than the $P_{\min}$, typically 20 kW. As in the case of low power, here, too, the nature of the spectrum of the SNL does not deviate much from the Kerr case. However the gain and the instability region marginally differs between the two. Figures 7(a) and 7(b) portray the instability spectrum at a power 20 kW for the conventional and SNL cases, respectively. One can observe that the gain of the band corresponding to $\kappa_1 = 0$ registers maximum and with an increase in κ_1 the gain decreases until the critical CCD, beyond which there appear two instability bands: One is near the center frequency and the other is the secondary band at higher detuning frequency. The critical CCD is found to be more than the case of the low power

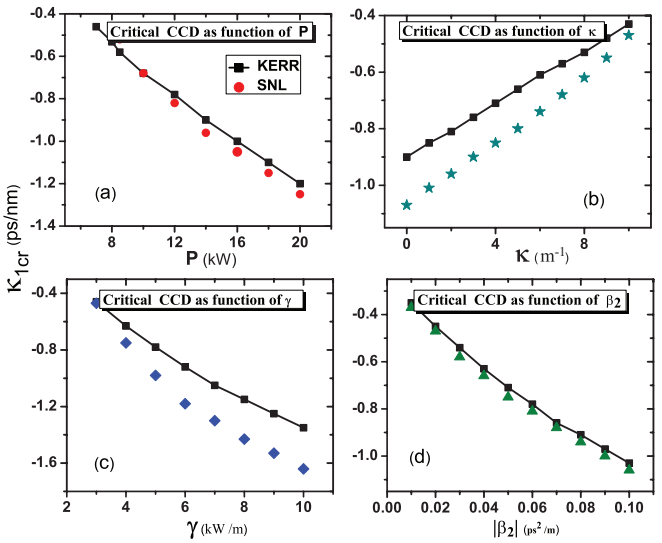

FIG. 8. (Color online) Illustration of the variation of critical CCD (κ_1**cr**) with system parameters in the anomalous dispersion regime. Parameters are $\beta_2 = -0.02$ ps^2 m^{-1}, $\gamma = 3.05$ kW $^{-1}$ m^{-1}, $P = 10$ kW, $\kappa = 10$ m^{-1}.

regime. In addition, the primary band near the center frequency possesses lower gain and the secondary band at higher detuning frequency features higher gain, which is identified as exactly opposite to the one that was observed for the lower power scheme. Further increase in CCD saturates the primary band and the gain of the secondary band constantly decreases.

A brief demonstration of the variation of κ_{1cr} as a function of the system parameter is shown in the Fig. 8. For the better manifestation, we consider both the conventional Kerr case and the SNL, to explicitly figure out the interplay between CCD and SNL in the instability spectrum. It is apparent from Fig. 8, the CCD corresponding to the splitting of the spectral band varies nearly linear. For instance, with an increase in the system parameters, such as power [Fig. 8 (a)], nonlinear coefficient [Fig. 8 (c)], and dispersion coefficient [Fig. 8(d)] the magnitude of κ_{1cr} ($|\kappa_{1cr}|$) increases, whereas κ decreases $|\kappa_{1cr}|$ as shown in Fig. 8. One can straightforwardly observe no significant change in the nature of the curve, which shows that at typical operating conditions both SNL and Kerr are closely related and similar in principles. However, although the nature of the curve is preserved in both cases, a slight change in the numerical value of the parameter is observed, which is inevitable owing to the different functional form of the nonlinear response. For instance, in all cases the magnitude of CCD (measured by $|\kappa_{1cr}|$) corresponding to SNL is slightly more than the conventional counterpart. It should be noted that our results are in complete agreement with the results of Ref. [47] at the limit $\Gamma \to 0$ and $\tilde{\gamma} \to \gamma$ corresponding to the conventional Kerr case.

Needless to say, the incorporation of SNL appears to bring no changes to the spectrum or to any additional new physics to the system. It should be noted, what has been discussed until now is with an assumption that the system is in the Type-I regime,($P < P_s$) and the dynamical behavior of SNL is identified to be in close proximity to the conventional Kerr case. Moving on to the higher power regime, typically

above the saturation power results in the Type-II regime, the SNL systems hold their signature and promise novel behavior. One such observation is system invariance at powers corresponding to the constant nonlinear factor. For example, consider the input power at the Type-I regime, typically $P = 8$ kW. The calculated nonlinear factor and the power threshold for sustained CW is given by 22.524 m^{-1} and 7.103 kW, respectively (refer to the formula discussed earlier). The power corresponding to the nonlinear factor equal to 22.524 m^{-1} in the Type-II regime is found to be 398.93 kW [value obtained from Fig. 3(b) at $\Gamma = 0.01\,kW^{-1}$]. The resulting P_{min} for the respective power is calculated to be equal to 354.281 kW. An insight observation of the relation between the power threshold for sustained CW and the input power reveals the existence of an interesting relation between P_{min} and P, that is, the ratio of the combination of the two powers in the two regimes is exactly equal to the ratio of the power threshold for CW. The relation can be written as $P^I/P^{II} = P^I_{min}/P^{II}_{min}$, and the superscript denotes the corresponding power regime (Type I or Type II). This shows that there exist two P_{min} at the two power regimes with constant nonlinear factor, against the constant P_{min} for the Kerr case. Interestingly, the MI spectrum corresponding to the power $P = 398.93$ kW in the Type-II regime is found to be exactly identical to Fig. 6(b); this shows that the system possesses two isolated powers at two regimes for any constant arbitrary value of nonlinear factor and becomes invariant at the particular powers. Similar behavior is observed at $P = 20$ kW (larger deviation from P_{min}); the nonlinear factor and P_{min} can take values, respectively, as 49.94 m^{-1} and 8.01 kW. The power corresponding to the nonlinear factor equal to 49.94 m^{-1} [evaluated from the curve in Fig. 3(b)] is found to be ≈ 286 kW and the calculated P_{min} is equal to 114.502 kW. As in the previous case, assuming input power equal to 286 kW leads to an identical spectrum similar to Fig. 7(b), and once again ensures the emphasized system invariance at two different powers. Thus, we conclude this section with this significant outcome and the underlined behavior is highlighted to be a signature of the SNL system.

B. Normal dispersion regime

This section corresponds to a particular case, where MI is generally proven to be impossible, owing to the lack of phase matching between the linear dispersive and nonlinear effects. The reason for this is the fact that, whenever the propagation of pulse is below the zero dispersion wavelength, then the dispersion coefficient takes a negative value. Therefore the delicate balance required for achieving the soliton or the MI between the dispersion and the self-focusing nonlinearity is not possible. However, MI is still proven to be possible in the normal dispersion regime with the aid of the higher-order dispersive effects, cross-phase modulations, and the delayed response. In the context of couplers or the two-core fibers, the presence of coupling between the two cores will extend the domain of MI to the normal dispersion regime as reported in Refs. [2,36,47,64].

Figure 9 depicts the instability spectrum for the Kerr and SNL cases. One can observe that both the Kerr case and SNL behave in a similar manner, except a slight modulation in the gain and the range of the unstable frequency, which

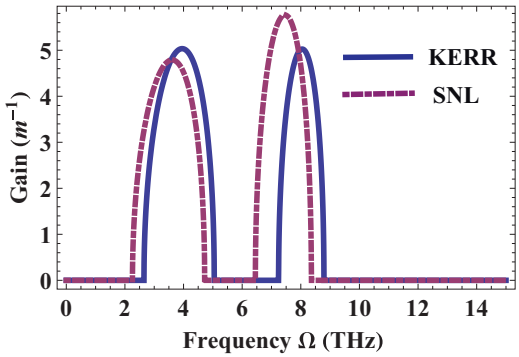

FIG. 9. (Color online) The instability spectra of Kerr and SNL in the normal dispersion regime at power $P = 10$kW. Parameters are $\beta_2 = 0.02\,ps^2\,m^{-1}, \gamma = 3.05\ kW^{-1}m^{-1}, \kappa = 10\,m^{-1}, \kappa_1 = 0\,ps\,m^{-1}$, and $\Gamma = 0.01\,kW^{-1}$.

is inevitable owing to the different functional form of the nonlinear response. To figure out the impact of pump power in the MI spectrum in the normal dispersion regime, first we consider zero CCD for the case of the conventional system, followed by the SNL case. Figure 10 shows the MI gain spectrum as a function of power at $\beta_2 = -0.02\,ps^2\ m^{-1}$ and $\kappa = 10\,m^{-1}$. At power $P = P_{min}$ a single broad instability band is observed at or near the center frequency. A slight increase in the pump power leads to two instability bands away from the center frequency and with an increase in the power the two instability bands drift towards the higher frequency side and the separation between the two instability band widens at higher powers. The gain of the instability band close to the center frequency increases and the band at higher detuning frequencies decreases with an increase in power. A continuous increase in power eliminates the band at the higher detuning frequency, and only one band survives. A similar behavior is observed for the case of SNL in the Type-I regime ($P < P_s$) as shown in the Fig. 11, except there is a slight change in the gain and the range of the unstable frequencies. However, what differentiates SNL from the conventional case is the

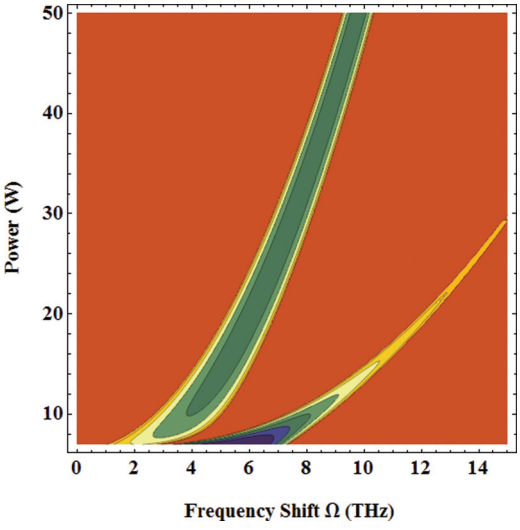

FIG. 10. (Color online) The contour plot showing the gain spectra of the Kerr case in the normal dispersion regime as a function of input power.

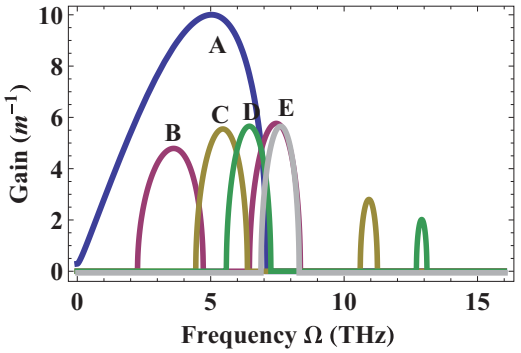

FIG. 11. (Color online) The instability spectra of the SNL system in the Type-I regime at different input powers $P(A = 7.035; B = 10; C = 20; D = 30; E = 50)$ kW.

Type-II regime, where one can straightforwardly observe from the Fig. 12, as power P is higher than the saturation power (typically, $P_s = 100$ kW) the two instability bands approach each other and a wide gap between the two instability bands is observed at $P = P_s = 100$ kW; this is interesting since it is exactly opposite to what has been observed in the Type-I case.

The influence of coupling coefficient in the instability spectrum at fixed power ($P = 20$ kW) is shown in Fig. 13 for different values of κ. At $\kappa = 0$, there is no instability band since there is no coupling between the two cores and the system resembles a conventional single-core fiber in the normal dispersion regime. Hence, the absence of the instability band is obvious since the system does not meet the much-required phase matching for the MI. Nonetheless, for any finite value of κ two instability bands arise, whose gains increase with an increase in κ before merging into a single broad band.

1. Interplay between CCD and SNL in the normal dispersion regime

We now switch to investigate the interplay between Γ and κ_1 in the MI spectrum. As in the case of the positive group dispersion coefficient, two different input powers are chosen: one near $P_{\min}$ and the other far from $P_{\min}$. For typical system parameters the $P_{\min}$ for Kerr and SNL is found to be 7 and 8 kW, respectively. Figures 14(a) and 14(b) show the instability spectrum at low input power corresponding to the Kerr and SNL systems. It is straightforward to notice that as

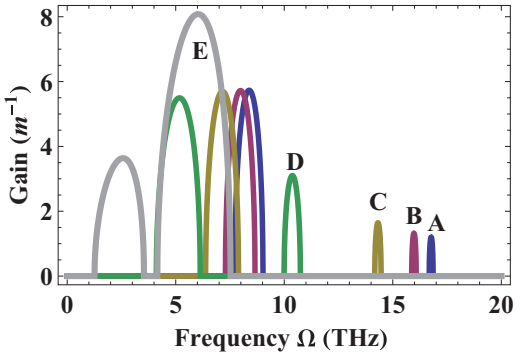

FIG. 12. (Color online) The instability spectra of the SNL system in the Type-II regime at different input powers $P(A = 100; B = 150; C = 200; D = 300; E = 400)$ kW.

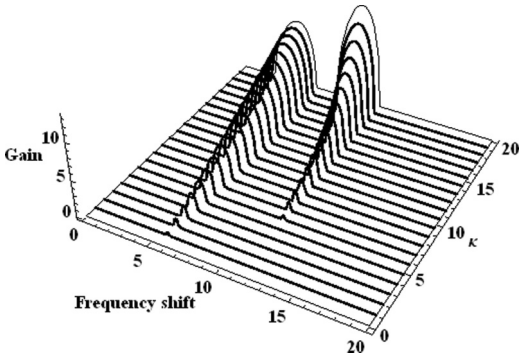

FIG. 13. The instability spectra of the SNL case as a function of coupling coefficient.

in the earlier cases, both Kerr and SNL in the Type-I regime closely resemble each other. It is apparent that there exist two instability bands at zero CCD, and with an increase in the value of the CCD the two instability bands approach each other and coalesce to form a single band of large gain and bandwidth. Similar to the earlier case of anomalous dispersion regime, here, too, there exists a critical CCD at which the dynamics evolves differently. However, the definition of critical CCD differs significantly from the anomalous dispersion case and it can be stated as the value of the CCD at which the coalesced

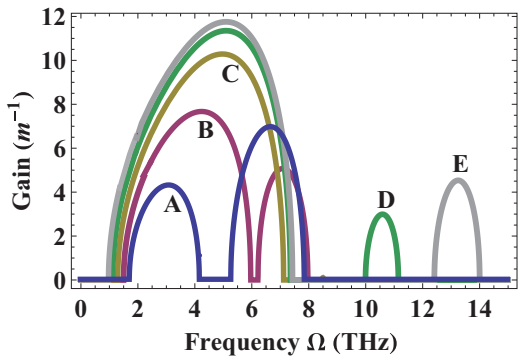

(a)

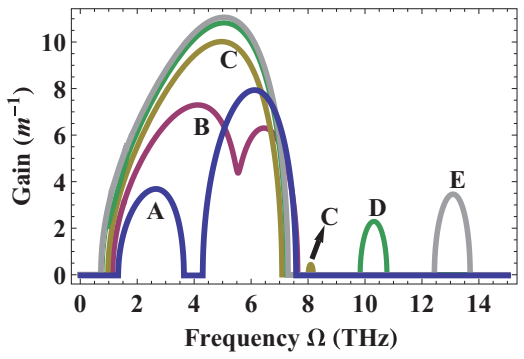

(b)

FIG. 14. (Color online) Plot showing the instability spectra at $P =$ 8 kW in the normal dispersion regime for different coupling coefficient dispersions $\kappa_1(A = 0; B = -0.2; C = -0.4; D = -0.6; E = -0.8)$ ps m^{-1}.(a) The MI spectra of Kerr at low power with the effect of coupling coefficient dispersion (κ_1). (b) The MI spectra of SNL at low power with the effect of coupling coefficient dispersion (κ_1).

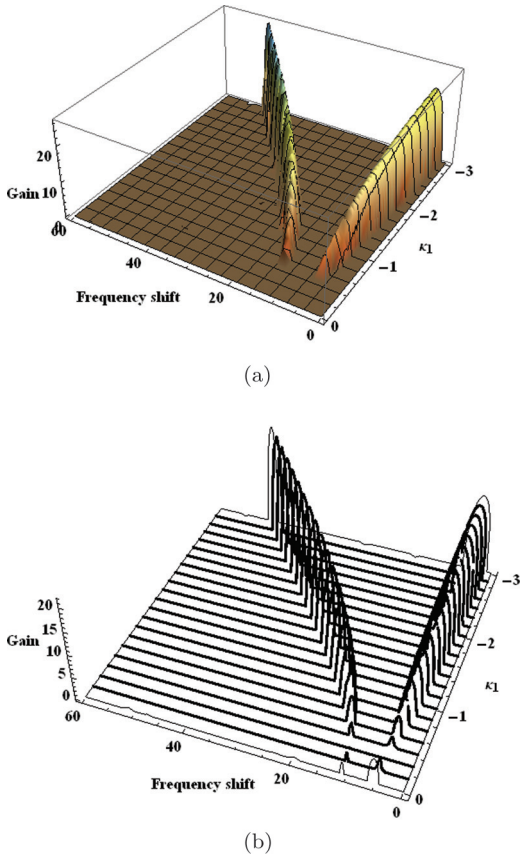

FIG. 15. (Color online) Plot showing the instability spectra at $P = 20$ kW in the normal dispersion regime for different coupling coefficient dispersions. (a) The MI spectra of Kerr at high power with the effect of coupling coefficient dispersion (κ_1). (b) The MI spectra of SNL at high power with the effect of coupling coefficient dispersion (κ_1).

band results in the reappearance of two instability bands. Thus for $\kappa_1 > \kappa_{1cr}$ the primary instability band near the center frequency registers maximum gain, and the secondary side band at higher detuning frequencies leads to continuous upshift whose gain increases with an increase in CCD.

Figures 15(a) and 15(b) represent the instability spectrum of the conventional and SNL cases at higher power, typically 20 kW, which is more than the $P_{\min}$. As in most cases, the SNL case does not bring new changes in the spectrum; the reasons are understandable since the SNL in the Type-I regime resembles closely the conventional Kerr case. However, the gain of the instability band in the SNL case is reduced, which is due to the inherent depletion in the nonlinear response of the SNL system.

Now we consider the pumping in the Type-II regime ($P > P_s$); the saturation power is fixed at 100 kW. It should be noted that the nonlinear factor is independent of the nature of the dispersion regime, therefore, the power corresponding to the constant nonlinear factor in the Type-II regime is the same as that for the anomalous dispersion regime. Thus, the system invariance at higher power above the power threshold is even observed in the normal dispersion regime. For an input power equal to 7 kW and 20 kW, the power corresponding to the constant nonlinear factor in the Type-II regime can be rewritten

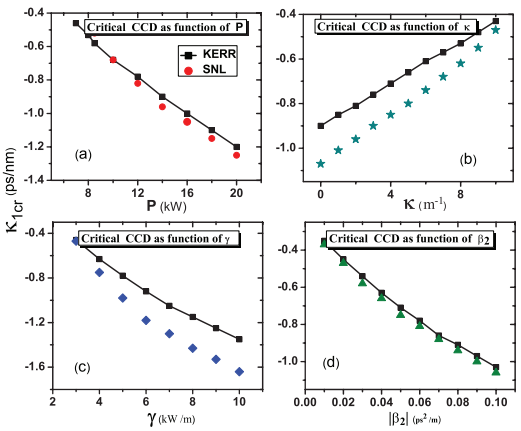

FIG. 16. (Color online) Plot showing the variation of critical CCD (κ_1**cr**) with system parameters in the normal dispersion regime. Parameters are $\beta_2 = 0.02$ ps^2 m^{-1}, $\gamma = 3.05$ kW $^{-1}$ m^{-1}, $P = 10$ kW, $\kappa = 10$ m^{-1}.

as 398.93 kW and 286 kW, respectively. It should be noted that for powers 354.281 kW and 286 kW the instability spectra resembles exactly Figs. 14(b) and 15(b), and thus emphasize the system invariance corresponding to the constant nonlinear factor.

To infer the influence of critical CCD in the instability spectrum, we have plotted critical CCD as a function of system parameters for both the conventional and the SNL case. As in the previous case, a near linear variation of critical CCD as a function of the system parameter is observed as shown in Fig. 16. One can readily observe that the nature of the curve is different from the anomalous dispersion case for both the conventional and SNL system, however, the conventional and SNL systems in the normal dispersion regime follow the same pattern with a slight difference in the numerical value. It is apparent from Fig. 16 that the magnitude of the critical CCD, $|\kappa_{1cr}|$ decreases with an increase in P [Fig. 16(a)] and γ [Fig. 16(c)] and increases with an increase in κ [Fig. 16(b)] and β_2 [Fig. 16(d)].

V. SUMMARY AND CONCLUSION

In summary, we have presented a theoretical investigation of MI in the twin-core fiber with the effect of saturation of the nonlinear response and coupling coefficient dispersion. The equation is suitably modeled to account for the SNL and CCD, thus the resulting equation can be used as a model equation for the highly nonlinear fibers such as semiconductor doped fibers, liquid core fibers, etc., An exact dispersion relation has been arrived using linear stability analysis and the detailed MI analysis is performed.

First, the symmetric or antisymmetric case is considered and it is observed that CCD does not dramatically modify the spectrum and SNL behaves in a perceptible manner such that the gain and the unstable region decreases. Hence, our spotlight is on the asymmetric case; first we studied the impact of various system parameters such as power and coupling coefficient in the instability spectrum. It is observed that with increase in power (coupling coefficient) the gain of the instability band increases (decreases) monotonously. For better insight, we

have divided the operating power regime as Type I and Type II, corresponding to input power below and above the saturation power. To illustrate, the conventional Kerr-type nonlinear response has also been considered alongside the SNL case. It is observed that both the Kerr and SNL cases behave similarly in the Type-I regime, but a slight decrease in the instability gain and frequency is observed for SNL, owing to the inherent depletion in the effective nonlinearity. On the other side of the picture, the Type-II regime behaves in the opposite way such that the increase in power above the saturation power leads to the suppression of MI by decreasing the gain and the unstable frequency window. To account for this interesting observation we plotted various system parameters such as nonlinearity, nonlinear factor, and power threshold for sustained CW as a function of power. It can be inferred from Fig. 3 that the SNL and Kerr cases play qualitatively in a different way under the influence of power. For instance, the nonlinearity and $P_{\min}$ is found to be independent of input power in the Kerr case, whereas both are functions of power in the SNL case. In addition, the product of effective nonlinearity and power is identified to be a crucial factor in all the observed effects and we called it the nonlinear factor. It is evident from Fig. 3(b) that the nonlinear factor increases monotonously for the Kerr case and behaves in a unique manner in the SNL system. It is observed that the nonlinear factor increases with an increase in power in the Type-I regime and reaches a maximum at $P = P_s$, and additional increase in power takes to the Type-II regime where the nonlinear factor progressively decreases. There exist two powers corresponding to the same nonlinear factor and the behavior of the system at the two respective powers is indeed the same, that is, the physical quantities, like the MI gain and the unstable frequency window, are preserved.

Following the detailed interpretation about the role of SNL in the MI spectrum, the subsequent section was dedicated to investigating the interplay between CCD and SNL in the anomalous dispersion regime. CCD leads to the emergence of a new spectral band; the number of bands, gain, and the unstable window are all characteristics of the value of the CCD. The saturation on the other hand inherently suppresses the MI by depleting the effective nonlinear coefficient. Basically, we consider two power schemes, one near and the other far from $P_{\min}$. Along similar lines as Ref. [47] for the Kerr case, the instability spectrum of the SNL case also differs at the two power schemes. The interesting observation is the existence of a critical CCD at which the system evolves in a different manner. For better insight, the critical CCD is plotted as a function of different system parameters such as power, coupling coefficient, nonlinear coefficient, and dispersion coefficient. A linear variation is observed for all the cases (refer to Fig. 8). An interesting feature which we speculate as unique in the system is the observation of system invariance at two different powers. Irrespective of the power scheme, the system remains invariant at two powers for the same nonlinear factor and the two powers are identified to be in two regimes, Type I and Type II, respectively. Furthermore, we extended the study to the case of the normal dispersion regime; it is obvious that MI generally is not feasible, however, the presence of the nonzero coupling coefficient ensures the required phase matching for MI. The behavior of MI in the normal dispersion regime differs a great deal from the anomalous dispersion case, such that two instability bands are observed against the single band in the anomalous dispersion regime. However, as in the anomalous case the gain of the SNL system is lesser than the conventional counterpart. As power increases the $P_{\min}$, two instability bands are observed and with an increase in power two bands drift away from the center frequency and at higher power only a single instability band survives. The coupling coefficient on the other hand behaves similarly as the power, such that any nonzero value of κ leads to two instability bands; it is worth noting that the instability band vanishes when κ equals zero, owing to the lack of phase matching for MI. The interplay between CCD and SNL is observed to be nearly the same as that of the anomalous dispersion case, except for the change in the definition of the critical CCD. Similar to the case of the anomalous dispersion regime, the system invariance is observed at two different powers.

Overall, the study based on the incorporation of saturation of the nonlinear response is interesting and offers a rich variety of information as follows: (i) the observation of the unique role of pump powers such that increasing power either increases or decreases the MI gain relative to the saturation power; (ii) the existence of two different powers for the same value of nonlinear factor; and (iii) the observation of the system invariance at two different powers. The above results are interesting and can pave the way for the design and development of twin-core fiber-based couplers, since one can maneuver the different characteristics of the fibers by merely tailoring the input power relative to the saturation power. Particularly, the observed unique role of pump power in the saturable system can revolutionize the dynamics of nonlinear directional couplers in such systems and can be useful in the ultrafast optical switching, power splitters, etc. Thus the present paper with the aforementioned results featuring the interplay between the SNL and CCD should be of good scientific value and we hope that our theoretical results can stimulate new experiments in the context of twin-core fibers.

ACKNOWLEDGMENTS

K.P. thanks Department of Science and Technology (DST), Department of Atomic Energy-Board of Research in Nuclear Sciences (DAE-BRNS), University Grants Commission (UGC), and Council of Scientific and Industrial Research (CSIR) Government of India, for financial support through major projects. K. Nithyanandan thanks CSIR, Government of India for providing financial support by awarding Senior Research Fellowship (SRF).

[1] G. Agrawal, *Nonlinear Fiber Optics*, 4th ed. (Academic Press, San Diego, 2007).
[2] G. Agrawal, *Application of Nonlinear Fiber Optics*, 2nd ed. (Academic Press, New York, 2001).
[3] T. B. Benjamin and J. E. J. Fier, Fluid Mechn. **27**, 417 (1967).
[4] V. I. Karpman, JETP Lett. **6**, 277 (1967).
[5] T. Taniuti and H. Washimi, Phys. Rev. Lett. **21**, 209 (1968).
[6] M. Lighthill, IMA J. Appl. Math. **1**, 269 (1965).

[7] L. A. Ostrovskii, Zh. Eksp. Teor. Fiz. **51**, 1189 (1966) [Sov. Phys.-JETP **24**, 797 (1967)].
[8] A. Hasegawa and F. Tappert, Appl. Phys. Lett. **23**, 142 (1973).
[9] J. M. Dudley, G. Genty, and S. Coen, Rev. Mod. Phys. **78**, 1135 (2006).
[10] R. V. Raja, K. Porsezian, and K. Nithyanandan, Phys. Rev. A **82**, 013825 (2010).
[11] A. Hasegawa and W. Brinkman, IEEE J. Quantum Electron. **16**, 694 (1980).
[12] M. Nakazawa, K. Suzuki, and H. A. Haus, IEEE J. Quantum Electron. **25**, 2036 (1989).
[13] M. Islam, S. Dijaili, and J. Gordon, Opt. Lett. **13**, 518 (1988).
[14] S. Trillo, S. Wabnitz, G. I. Stegeman, and E. M. Wright, J. Opt. Soc. Am. B **6**, 889 (1989).
[15] K. Hammani, B. Wetzel, B. Kibler, J. Fatome, C. Finot, G. Millot, N. Akhmediev, and J. M. Dudley, Opt. Lett. **36**, 2140 (2011).
[16] M. N. Z. Abouou, P. T. Dinda, C. M. Ngabireng, B. Kibler, and F. Smektala, J. Opt. Soc. Am. B **28**, 1518 (2011).
[17] K. Tai, A. Hasegawa, and A. Tomita, Phys. Rev. Lett. **56**, 135 (1986).
[18] R. Malendevich, L. Jankovic, G. Stegeman, and J. S. Aitchison, Opt. Lett. **26**, 1879 (2001).
[19] M. F. Shih, C. C. Jeng, F. W. Sheu, and C. Y. Lin, Phys. Rev. Lett. **88**, 133902 (2002).
[20] S. Wen and D. Fan, J. Opt. Soc. Am. B **19**, 1653 (2002).
[21] M. Saffman, G. McCarthy, and W. Krolikowski, J. Opt. B **6**, S397 (2004).
[22] J. D. Harvey, R. Leonhardt, S. Coen, G. K. L. Wong, J. Knight, W. J. Wadsworth, and P. S. Russell, Opt. Lett. **28**, 2225 (2003).
[23] S. Pitois and G. Millot, Opt. Commun. **226**, 415 (2003).
[24] P. Dinda and K. Porsezian, J. Opt. Soc. Am. B **27**, 1143 (2010).
[25] T. Tanemura, Y. Ozeki, and K. Kikuchi, Phys. Rev. Lett. **93**, 163902 (2004).
[26] G. P. Agrawal, Phys. Rev. Lett. **59**, 880 (1987).
[27] K. Nithyanandan, R. V. J. Raja, K. Porsezian, and B. Kalithasan, Phys. Rev. A **86**, 023827 (2012).
[28] E. Seve, P. TchofoDinda, G. Millot, M. Remoissenet, J. M. Bilbault, and M. Haelterman, Phys. Rev. A **54**, 3519 (1996).
[29] G. Millot, E. Seve, S. Wabnitz, and J. M. Haelterman, J. Opt. Soc. Am. B **15**, 1266 (1998).
[30] G. I. Stegeman, E. M. Wright, N. Finlayson, R. Zanoni, and C. T. Seaton, J. Lightwave Technol. **6**, 953 (1988).
[31] K. R. Khan, T. X. Wu, D. N. Christodoulides, and G. I. Stegeman, Opt. Express **16**, 9417 (2008).
[32] K. Kitayama and S. Wang, Appl. Phys. Lett. **43**, 17 (1983).
[33] P. Ramos and C. Paiva, IEEE J. Quantum Electron. **35**, 983 (1999).
[34] M. Koys, I. Bugar, V. Mesaros, F. Uherek, and R. Buczynski, Proc. SPIE **7746** (2010), doi: 10.1117/12.882890.
[35] A. Betlej, S. Suntsov, K. G. Makris, L. Jankovic, D. N. Christodoulides, G. I. Stegeman, J. Fini, R. T. Bise, and D. J. DiGiovanni, Opt. Lett. **31**, 1480 (2006).
[36] R. Tasgal and B. Malomed, Phys. Scr. **60**, 418 (1999).
[37] A. W. Snyder, J. Opt. Soc. Am. **62**, 1267 (1972).
[38] K. Chiang, J. Opt. Soc. Am. B **14**, 1437 (1997).
[39] Z. Wang, T. Taru, T. A. Birks, J. C. Knight, Y. Liu, and J. Du, Opt. Express **15**, 4795 (2007).
[40] K. Saitoh, Y. Sato, and M. Koshiba, Opt. Express **11**, 3188 (2003).
[41] S. Zhang, X. Yu, Y. Zhang, P. Shum, Y. Zhang, L. Xia, and D. Liu, IEEE Photonics Journal **4**, 1178 (2012).
[42] M. Liu and P. Shum, IEEE Photonics Technol. Lett. **16**, 1080 (2004).
[43] M. Liu, D. Li, and Z. Liao, JETP Lett. **95**, 10 (2012).
[44] Q. Li, Y. Xie, Y. Zhu, and S. Qian, Opt. Commun. **281**, 2811 (2008).
[45] K. S. Chiang, Y. T. Chow, D. J. Richardson, D. Taverner, L. Dong, L. Reekie, and K. M. Lo, Opt. Commun. **143**, 189 (1997).
[46] P. Peterka, P. Honzatko, J. Kanka, V. Matejec, and I. Kasik, Proc. SPIE **5036**, 376 (2003).
[47] J. H. Li, K. S. Chiang, and K. W. Chow, J. Opt. Soc. Am. B **28**, 1693 (2011).
[48] G. Stegeman, C. Seaton, C. Ironside, T. Cullen, and A. Walker, Appl. Phys. Lett. **50**, 1035 (1987).
[49] E. Caglioti, S. Trillo, S. Wabnitz, B. Daino, and G. Stegeman, Appl. Phys. Lett. **51**, 293 (1987).
[50] Y. Chen, Electron. Lett. **26**, 1374 (1990).
[51] Y. Chen, J. Opt. Soc. Am. B **8**, 986 (1991).
[52] P. Khadzhi and O. Orlov, Tech. Phys. **45**, 1164 (2000).
[53] U. Langbein, F. Lederer, T. Peschel, and H.-E. Ponath, Opt. Lett. **10**, 571 (1985).
[54] J.-L. Coutaz and M. Kull, J. Opt. Soc. Am. B **8**, 95 (1991).
[55] R. Zhang, J. Teipel, and H. Giessen, Opt. Express **14**, 6800 (2006).
[56] H. Zhang, S. Chang, J. Yuan, and D. Huang, Optik **121**, 783 (2010).
[57] T. Uthayakumar, R. Raja, and K. Porsezian, J. Lightwave Technol. **30**, 2110 (2012).
[58] S. Pricking, M. Vieweg, and H. Giessen, Opt. Express **19**, 21673 (2011).
[59] C. Ping Yu, J. Hong Liou, S. Shuo Huang, and H. Chun Chang, Opt. Express **16**, 4443 (2008).
[60] S. Gatz and J. Herrmann, J. Opt. Soc. Am. B **8**, 2296 (1991).
[61] J. M. Hickmann, S. B. Cavalcanti, N. M. Borges, E. A. Gouveia, and A. S. Gouveia-Neto, Opt. Lett. **18**, 182 (1993).
[62] J. Herrmann, J. Opt. Soc. Am. B **8**, 1507 (1991).
[63] Y.-F. Chen, K. Beckwitt, F. W. Wise, B. G. Aitken, J. S. Sanghera, and I. D. Aggarwal, J. Opt. Soc. Am. B **23**, 347 (2006).
[64] S. Trillo and S. Wabnitz, J. Opt. Soc. Am. B **6**, 238 (1989).